Jesus Calvo-Castrp, Sebastian Macza, Connor Thomson, Graeme Morris, Alan R. Kennedy and Callum J. McHugh, 'Twist and shout:  a surprising synergy between aryl and *N*-substituents defines the computed charge transport properties in a series of crystalline diketopyrrolopyrroles', *CrysEngComm*, Vol 18(48):  9382-9390, first published online 22 November 2016, available at doi:  10.1039/C6CE02261H

Journal Name

ARTICLE

# *Twist and Shout*: A surprising synergy between aryl and N-substituents defines the computed charge transport properties in a series of crystalline diketopyrrolopyrroles

Received 00th January 20xx,
Accepted 00th January 20xx

DOI: 10.1039/x0xx00000x

**www.rsc.org/**

Jesus Calvo-Castro,* [c] Sebastian Maczka,[a] Connor Thomson, [a] Graeme Morris, [a] Alan R. Kennedy, [b] and Callum J. McHugh*[a]

The influence of sytematic variation of aryl and N-substitution on predicted charge transport behaviour in a series of crystalline diketopyrrolopyrroles is evaluated. A correct combination of substituents is revealed to maximise those properties which dictate device performance in organic single crystals based upon this structural motif. For electron transport, furan and N-alkyl substitution emerge as optimal molecular design strategies, whilst phenyl structures bearing N-benzyl substituents are shown to offer the most significant promise as highly sought after crystalline hole transport materials.

## Introduction

In crystalline charge mediating organic materials, control of molecular solid state aggregation and π-π stacking can exert a dramatic impact on intermolecular electronic properties which define delocalised band transport and localised, thermally activated hopping of charge carriers.[1-4] Electronic coupling, or charge transfer integrals for hole/electron transport, $t_{h/e}$, describe the extent of wavefunction overlap and are related to the strength of the π-π interactions between molecules and play a significant role in either description.[5-7] Inner-sphere reorganisation energy for holes/electrons, $\lambda_{h/e}$, characterises the change in energy between charged and neutral molecular states, owing to geometrical relaxation of the localised molecular environment and can be detrimental to transport behaviour when charge hopping is predominant. Large intermolecular interaction energies, $\Delta E_{CP}$, are highly desirable in organic semiconductors to preserve the integrity of crystalline intermolecular interactions involving π-π stacking, and to perpetuate band structure. Thermally-induced slippage of π-π stacking domains can result in considerable variation in $t_{h/e}$, which can ultimately be detrimental to carrier mobility. Regardless of the mechanism of charge transport involved however, it is generally accepted that an increase in electronic coupling, $t_{h/e}$, minimal electron-phonon coupling, $\lambda_{e/h}$ and large values of $\Delta E_{CP}$ are desirable.[5, 8, 9]

Diketopyrrolopyrrole (DPP) based materials are exciting charge transfer mediators, with high mobilities reported in organic field effect transistors (OFETs).[10-26] Our group are engaged in the rational design of crystalline and thin film DPP architectures[27-33] and have demonstrated in a number of phenyl core-substituted N-benzyl DPPs that small structural variations, particularly involving halogenation, can profoundly influence supramolecular packing via manipulation of single crystal intermolecular interactions.[28, 29, 31, 32] We have pioneered the application of Truhlar's M06-2X density functional in the theoretical analysis of charge transfer integrals, reorganisation energies and interaction energetics in DPPs,[27-33] many of which are comparable or supersede those computed for the single crystal structures of state of the art organic semiconductors such as rubrene.[29] The M06-2X semilocal density functional has been shown to quantitatively agree with state-of-the-art quantum mechanical calculations describing non-covalent interactions through its inclusion of important medium distant London dispersion forces.[34, 35]

All of the DPP single crystal structures reported by us previously involve core phenyl substituents and incorporate N-benzyl substitution of the lactam nitrogen atoms. It is widely perceived in the literature that phenyl DPPs should display poor charge transport behaviour as a consequence of deviation from planarity of their core phenyl/lactam dihedral angles and as a result they are usually overlooked in favour of more elaborate heteroaromatic structures.[36-39] It is proposed that conjugated backbone twists in N-alkylated phenyl DPPs are detrimental to the formation of

[a] *School of Science and Sport, University of the West of Scotland, Paisley, PA1 2BE, UK.*
[b] *Department of Pure & Applied Chemistry, University of Strathclyde, Glasgow, G1 1XL, UK.*
[c] *School of Life and Medical Sciences, University of Hertfordshire, Hatfield, AL10 9AB, UK.*

Electronic Supplementary Information (ESI) available: Full details regarding the preparation, characterisation, crystallographic analysis and theoretical modelling of reported compounds. See DOI: 10.1039/x0xx00000x

strong solid state π-π interactions and that their flexibility also contributes to an increase in inner sphere reorganisation energy.[36] Thus, significant effort has been placed on development of chalcogen based DPPs with core phenyl rings replaced by planar thiophene, furan or selenophene groups.[36-39] We are however, not aware of any studies which critically evaluate charge transfer integrals, interaction energetics or reorganisation energies in the design of heteroaromatic DPPs and their phenyl equivalents. In addition, there have been no reports in the literature of heteroaromatic DPPs incorporating N-benzyl substitution in their molecular design.

Motivated by these shortcomings, in the present study, we systematically examine the influence of core aryl and N-substitution on the electronic behaviour predicted from a series of experimentally determined DPP single crystal structures. We report the preparation and characterisation of new thiophene and furan N-benzyl DPP single crystal structures and compare their intrinsic supramolecular packing behaviour to phenyl and N-(*n*-hexyl) equivalents. Through consideration of computed interaction energies, $\Delta E_{CP}$, charge transfer integrals, $t_{h/e}$, and reorganisation energies, $\lambda_{h/e}$, as determined from the crystal extracted π-π stacks and their molecular geometries, it is clear that the correct combination of aromatic and N-substituents is crucial in order to maximise those properties which can influence overall charge transport behaviour in these molecular crystals.

## Results and Discussion

### Synthesis and single crystal structure description

Novel N-benzylated thiophene and furan DPPs were obtained according to Scheme 1 and their structures determined by single crystal X-ray diffraction (ESI). Synthesis[20, 29, 40, 41] and single crystal structures[29, 39, 41, 42] of the phenyl N-benzyl DPP and N-(*n*-hexyl) equivalents have been reported previously. In the present study, the six structures, ***PBDPP***, ***TBDPP***, ***FBDPP***, ***PADPP***, ***TADPP*** and ***FADPP*** (CCDC numbers 980388, 1506132, 1506131, 786510, 737422 and 1440140 respectively) were adorned names in the form of XYDPP, arising from their topology, where X and Y represent substitution of the central DPP core (***P*** = phenyl, ***T*** = thiophene, ***F*** = furan) and nitrogen atoms (***B*** = benzyl, ***A*** = *n*-hexyl) respectively.

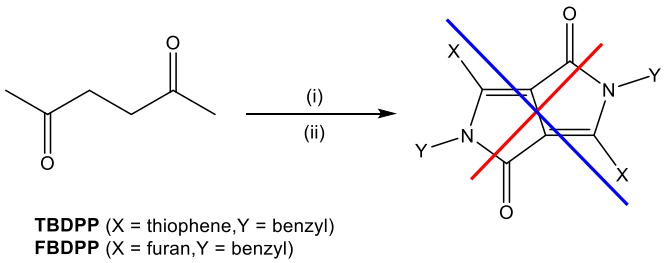


**TBDPP** (X = thiophene,Y = benzyl)
**FBDPP** (X = furan,Y = benzyl)

**Scheme 1 XDPP** Synthetic Route. (i) $C_4H_3SCN$ or $C_4H_3OCN$, Na, *t*-amyl alcohol, reflux; (ii) BnBr, $K_2CO_3$, DMF, 120 °C. Blue and red solid lines illustrate the DPP long, Δx and short, Δy molecular axes respectively.

All of the structures are characterised by molecules with crystallographically imposed centrosymmetry. In each case, cofacial π-π stacking domains are exhibited, propagating along the respective crystal axes as illustrated in Figure 1 and Table 1. The phenyl and furan structures (***PADPP***, ***PBDPP***, ***FADPP*** and ***FBDPP***) and the N-alkyl thiophene derivative, ***TADPP***, display 1-dimensional π-π stacking regimes; with π-π dimer topology that is dependent on aryl and N-substituents. Surprisingly to us, the N-benzyl thiophene structure, ***TBDPP***, is different from the other structures in the series in that it exhibits 2-dimensional π-π stacking, with the emergence of a cruciform arrangement of the π-π stacking dimers, similar to that reported by us previously for a fluorinated phenyl substituted DPP[59] (Figure 2). Unlike the fluorinated species however, the orthogonal π-π stacking dimer propagating along the crystallographic *b*-axis in ***TBDPP*** is extremely slipped and accordingly we predict reduced wavefunction overlap and a lower transfer integral from this particular π-π stacking motif.

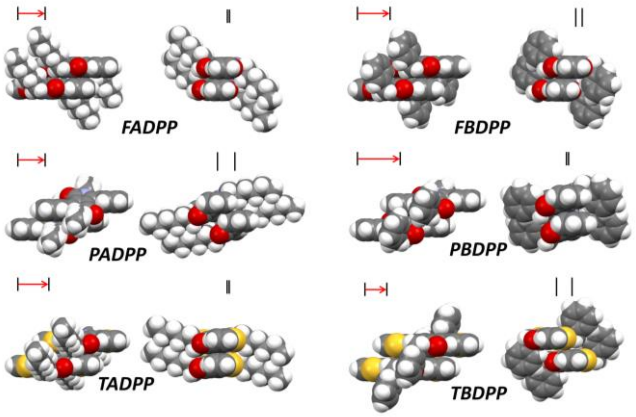


**Figure 1** Illustration of displacements along the long molecular axis, Δx (left) and short molecular axis, Δy (right) for each of the investigated DPP architectures

**Table 1** Features of crystal extracted π-π stacking dimers

| System | Δx / Å | Δy / Å | Δz / Å | π-π stacking axis | Space group |
|---|---|---|---|---|---|
| ***PADPP*** | 3.57 | 2.32 | 3.54 | b | $P2_1/c$ |
| **PBDPP** | 4.52 | 0.05 | 3.44 | a | P-1 |
| **FADPP** | 3.57 | 0.15 | 3.31 | b | C2/c |
| **FBDPP** | 4.11 | 1.78 | 3.38 | b | C2/c |
| **TADPP** | 4.04 | 0.05 | 3.53 | b | $P2_1/c$ |
| **TBDPP** | 2.96 | 3.26 | 3.45 | a | $P2_1/n$ |

Slipped cofacial π-π stacking behaviour is often regarded as a key structural feature leading to the emergence of semiconductor bands in organic materials.[34, 43, 44] In the single crystal structures described herein, the degree of long and short molecular axis slip and inter-dimer separation is markedly variable, which we attribute to the combined influence of the DPP core aryl and N-substituents in each case. Accordingly, in the phenyl substituted structures, N-benzylation in ***PBDPP*** versus N-alkylation in ***PADPP*** affords a reduction in both the short molecular axis π-π dimer slip (Δy = 0.05 and 2.32 Å for ***PBDPP*** and ***PADPP*** respectively) and in the inter-dimer separation (Δz = 3.44 and 3.54 Å for ***PBDPP*** and ***PADPP*** respectively); but increases the long molecular axis π-π dimer slip from Δx = 3.57 Å in ***PADPP*** to Δx = 4.52 Å in ***PBDPP***. In each of the furan based architectures, we find that N-benzyl substitution is detrimental to a close π-π dimer configuration, and is responsible for an increase in the long and short molecular axes slip and the inter-dimer separation compared with the equivalent N-alkylated structure. For the thiophene based analogues, the impact of N-substitution is in stark contrast to the behaviour observed in the phenyl equivalents. We note that N-benzylation in this case actually affords a considerable increase in the short molecular axis slip (Δy = 0.05 and 3.26 Å for ***TADPP*** and ***TBDPP*** respectively), whilst at the same time facilitates a significant reduction in the long molecular axis slip (Δy = 4.04 and 2.96 Å for ***TADPP*** and ***TBDPP*** respectively) compared to N-alkylation. In the thiophene structures, N-benzylation also exerts a positive influence on inter-dimer separation, with Δz = 3.45 Å in ***TBDPP*** compared to Δz = 3.53 Å in ***TADPP***. It is clear, as discussed by us previously,[28, 29, 31, 32] when engineering π-π stacking dimer interactions and their spatial overlap in DPP single crystals to maximise wavefunction overlap and electronic coupling between monomers, that careful consideration of both the core aryl and N-substituents is required (vide infra).

The dihedral angle between core aryl rings and the DPP central core was determined for each structure. It was observed in line with previous reports,[36] that regardless of substitution on the lactam nitrogen atoms, phenyl based systems always exhibit greater dihedral angles than their near-planar thiophene and furan equivalents (32.7/22.5(2), 0.6/1.0(5) and 9.1/3.7(4) ° for ***PADPP***/***PBDPP***, ***FADPP***/***FBDPP*** and ***TADPP***/***TBDPP*** respectively). The lower dihedral angles observed in thiophene and furan containing motifs are associated with a greater number of stabilising intramolecular interactions compared to the phenyl substituted equivalents. Close intramolecular interactions between the electronegative chalcogen atoms and electropositive methylene hydrogen atoms were observed in the thiophene and furan systems (H---S/O = 2.37/2.42 and 2.55/2.51 Å for ***FADPP***/***FBDPP*** and ***TADPP***/***TBDPP*** respectively). In addition, relative positions of the benzyl and alkyl N-substituents with respect to the plane of the DPP core were investigated. We observed that in all cases, benzyl groups exhibit lower dihedral angles than their alkyl equivalents (110.9/102.4(2), 95.9/79.0(3) and 95.6/81.7(3) ° for ***PADPP***/***PBDPP***, ***FADPP***/***FBDPP*** and ***TADPP***/***TBDPP*** respectively).

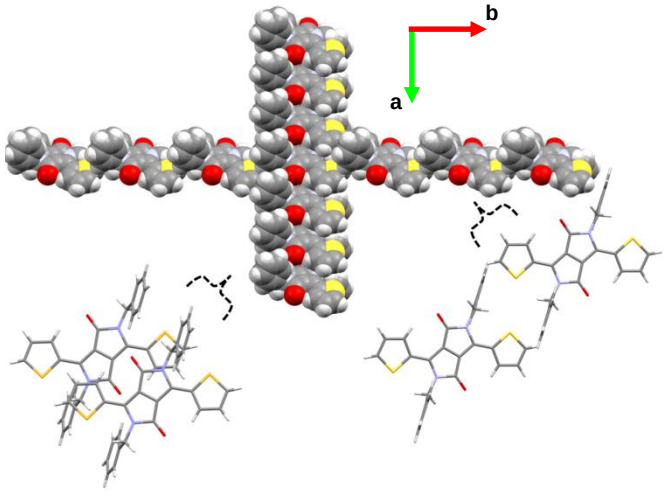


**Figure 2** ***TBDPP*** cruciform π-π stacking arrangement (centre space filled representation) illustrating slipped π-π dimer configurations (crystallographic axes are labelled)

**Substituent effects on intermolecular interactions for nearest neighbouring dimer pairs**

We have previously reported a DPP model system describing the energetic profile observed when two fully planar non N-substituted phenyl DPP monomers are displaced with respect to one another from a fully eclipsed geometry across their long molecular axes (Δx).[28, 29] Herein, we applied this approach to equivalent thiophene (**TDPP**) and furan (**FDPP**) 1-dimensional flyby analyses using the M06-2X density functional at the 6-311G(d) level. Systematic variation of the intermolecular displacement (Δx) between planar thiophene and furan monomers was measured across a distance of 15.3 Å in 0.3 Å increments while retaining Δy = 0.0 Å and restricting the optimised Δz distance between dimers to 3.6 Å. Remarkably, the potential energy surfaces (PES) of both the thiophene and furan models replicate that obtained from the phenyl system, **PDPP** (**HDPP** in the original publications)[28, 29] almost entirely, with the same number of energy minima observed at the same approximate long molecular axis (Δx) position

and consistent with their similar frontier molecular orbital surfaces (Figure 3).

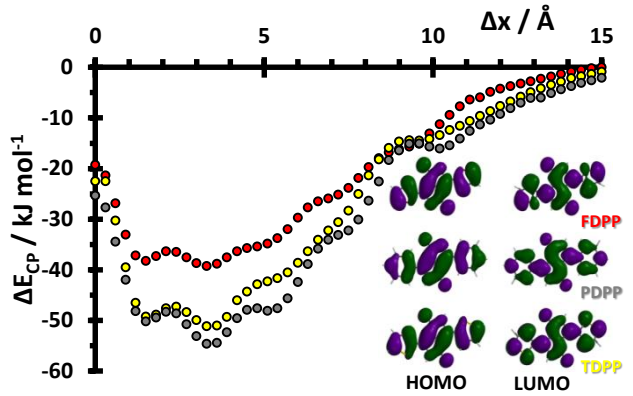


**Figure 3** Counterpoise corrected interaction energies for **FDPP** (red), **PDPP** (grey) and **TDPP** (yellow) as a function of intermolecular slip, Δx and computed frontier molecular orbitals (insert), M06-2X/6-311G(d)

We report global thiophene and furan energy minima corresponding to ca. Δx = 3.3 Å and local minima for both at ca. Δx = 1.5, 5.1, 7.5 and 10.0 Å. Regardless of aryl substituent, for N-benzyl structures, we find that crystal derived π-π dimer long molecular axis slip is centred close to the predicted PES global minimum (4.52, 2.96 and 4.11 Å for ***PBDPP***, ***TBDPP*** and ***FBDPP*** respectively). It is noteworthy, particularly for the thiophene and furan N-benzyl analogues, that despite a constrained short molecular axis slip of Δy = 0.0 Å in the model systems, the most stable thiophene and furan model dimer predictions are consistent with their respective π-π crystal structure geometries, where a substantial increase in short molecular axis slip is observed in both of the π-π dimers compared to the corresponding phenyl equivalent (Δy = 0.05, 3.26 and 1.78 Å for ***PBDPP***, ***TBDPP*** and ***FBDPP*** respectively). For the N-alkyl structures, thiophene and furan analogues are well represented by their model dimers, where a reduced short molecular axis slip (Δy = 0.15 and 0.05 Å for ***FADPP*** and ***TADPP*** respectively) predominates and the experimentally observed long molecular axis slip lies close to the predicted PES global minimum (Δx = 3.57 and 4.04 Å for ***FADPP*** and ***TADPP*** respectively). In the corresponding phenyl structure, despite an increase in short molecular axis slip as a result of N-alkylation (Δx = 2.32 Å in ***PADPP*** compared with Δx = 0.05 Å in ***PBDPP***) the observed long molecular axis slip (Δx = 3.57 Å) is also consistent with the theoretical global minimum.

The influence of core-DPP aryl and N-substitution on the intermolecular interactions of crystal derived nearest neighbour dimer pairs was investigated for each of the structures (specific dimers are denoted in Roman numerals with reference to ESI). Consistently larger intermolecular interaction energies were computed when comparing N-benzylation to N-alkylation. In considering N-benzylated structures, the largest total intermolecular interaction energy (Table 2) was observed for ***PBDPP*** and the lowest for ***TBDPP*** (-294.7, -267.1 and -259.6 kJ mol$^{-1}$ for ***PBDPP***, ***FBDPP*** and ***TBDPP*** respectively); despite it exhibiting a greater number of nearest neighbouring dimer pairs (10, 12 and 14 neighbours for ***FBDPP***, ***PBDPP***, and ***TBDPP*** respectively). The low intermolecular interaction energy of ***TBDPP*** is consistent with the small computed interaction energies for each of its nearest neighbour dimer pairs, with the exception of the π-π stacking dimer pair (III), which is equivalent in energy to the π-π stacking dimers of ***PBDPP*** and ***FBDPP*** (-70.12, -74.47 and -78.53 kJ mol$^{-1}$ for ***PBDPP*** (VI), ***TBDPP*** (III) and ***FBDPP*** (IV) respectively). The relative ordering of the computed intermolecular interactions for these π-π dimer pairs is consistent with their degree of displacement along the long molecular axis as summarised in Table 1.

For the N-alkylated structures, furan substitution of ***FADPP*** affords the largest intermolecular interaction energy (-250.28 kJ mol$^{-1}$), with comparable energies observed in both the phenyl and thiophene structures (-212.12 and -212.40 kJ mol$^{-1}$ for ***PADPP*** and ***TADPP*** respectively). Increased stabilisation of ***FADPP*** can be accounted for on the basis of a greater number of nearest neighbours dimer pairs and π-π stacking dimer energy compared with ***TADPP*** and ***PADPP*** respectively.

To develop an understanding of substituent effects on dimer stability we computed the intermolecular interaction energies for a series of cropped dimers where aryl and N-substituents were removed (Table 2). For the N-benzyl structures, significant destabilisation was observed in the overall interaction energy of ***PBDPP*** upon removal of either phenyl or benzyl substituents, with each making a similar contribution to the overall stability (186.6 and 188.7 kJ mol$^{-1}$ respectively). In the thiophene system, ***TBDPP***, we observed a greater degree of destabilisation on removal of the N-benzyl substituents compared with the thiophene rings (195.1 kJ mol$^{-1}$ versus 163.3 kJ mol$^{-1}$), whilst the opposite behaviour was observed for the furan equivalent, ***TBDPP*** (136.6 kJ mol$^{-1}$ versus 159.2 kJ mol$^{-1}$). Of surprise to us was the very small DPP-core to DPP-core stabilisation computed for the nearest neighbour dimer pairs in each of the N-benzyl derivatives, particularly for the thiophene-containing structural motif (-26.18, -3.12 and -24.5 kJ mol$^{-1}$ for ***PBDPP***, ***TBDPP*** and ***FBDPP*** respectively).

For N-alkylated systems, we observed that in all cases, removal of the N-alkyl substituents on progression from ***XYDPP*** to structurally modified **XDPP** systems was less destabilising compared with the equivalent N-benzyl structures. The opposite behaviour, to a lesser extent in ***FADPP***, was observed upon progression from ***XYDPP*** to **YDPP**, where the interaction energy was more significantly reduced upon removal of the core aryl rings. This behaviour is attributed to a larger contribution of the π-π stacking dimer energy to the overall interaction energy in the N-alkyl systems, which is lost upon removal of the aryl substituents. Likewise, removal of the N-alkyl groups has a diminished impact on the total energy compared with the N-benzyl substituents as the alkyl groups do not contribute as much to the total energy in all of the nearest neighbour dimers pairs (see ESI).

**Table 2** Sum of counterpoise corrected intermolecular interaction energies, $\Delta E_{CP}$, for modified and unmodified nearest neighbour dimer pairs

| | $\Delta E_{CP}$ / kJ mol$^{-1}$ | | | | | |
|---|---|---|---|---|---|---|
| **System** | ***PADPP*** | ***PBDPP*** | ***TADPP*** | ***TBDPP*** | ***FADPP*** | ***FBDPP*** |
| ***XYDPP*** | -212.12 | -294.70 | -212.40 | -259.60 | -250.28 | -267.14 |
| **XDPP** | -141.30 | -108.10 | -111.46 | -64.50 | -152.78 | -130.50 |
| **YDPP** | -41.52 | -106.00 | -56.46 | -96.32 | -95.60 | -107.86 |
| **DPP** | -11.66 | -26.18 | -22.12 | -3.12 | -28.32 | -24.50 |

**Influence of aryl and N-substituents on computed π-π stacking dimer intermolecular interaction energies**

Given the importance of π-π stacking dimers in defining the charge transport behaviour of organic semiconductors,[34, 43, 44] the role of systematic aryl and N-substitution in stabilising crystal derived π-π dimer pairs in each of the reported structures was evaluated (Table 3). In all cases, N-benzylated systems were observed to surpass the computed intermolecular interactions compared with their alkylated counterparts, thus reinforcing our previous assertion regarding the positive role of benzyl substitution in enhancing the thermal stability of π-π stacking dimer pairs in DPP single crystals.[28, 29, 31, 32]

We report for the phenyl substituted systems, ***PADPP*** and ***PBDPP***, that removal of either the alkyl or benzyl groups affords ca. 40% destabilisation of the total binding energy for the π-π stacking dimer pairs. This effect can be attributed to an electrostatic intermolecular interaction between electropositive methylene protons and electronegative carboxylic oxygen atoms situated 2.85 Å apart in ***PBDPP*** and to a stabilising dispersive interaction between the aliphatic $C_6$ chains and DPP core phenyl rings in ***PADPP*** (Figure 4). Despite a larger displacement along the short molecular axis in ***PADPP***, it is interesting to note that on removal of the phenyl rings there is a clear increase in destabilisation observed in the alkylated analogue ($\Delta E_{CP}$ = -59.94/-10.90 and -70.12/-28.58 kJ mol$^{-1}$ for ***XYDPP***/**YDPP** dimer pairs of ***PADPP*** and ***PBDPP*** respectively). We associate the latter to a combination of a slipped-cofacial intermolecular interaction between the core phenyl rings and dispersive interactions between the core phenyl rings and alkyl chains, favoured by the closer alignment along the long molecular axis observed in ***PADPP*** compared to its benzylated equivalent. The differences in the computed intermolecular interactions for the artificially generated DPP cropped dimer pairs for ***PADPP*** and ***PBDPP*** can be readily understood as a result of differing displacements along their short molecular axes (vide supra).

**Table 3** Counterpoise corrected intermolecular interaction energies, $\Delta E_{CP}$, for modified and unmodified π-π stacking dimer pairs

| | $\Delta E_{CP}$ / kJ mol$^{-1}$ | | | |
|---|---|---|---|---|
| **System** | ***XYDPP*** | **XDPP** | **YDPP** | **DPP** |
| ***PADPP*** | -59.94 | -33.21 | -10.90 | -3.77 |
| ***PBDPP*** | -70.12 | -41.89 | -28.58 | -12.12 |
| ***TADPP*** | -65.45 | -51.13 | -18.95 | -12.66 |
| ***TBDPP*** | -74.47 | -27.26 | -35.48 | -2.18 |
| ***FADPP*** | -72.00 | -56.58 | -24.72 | -12.91 |
| ***FBDPP*** | -78.53 | -45.11 | -34.25 | -12.01 |

It is important to note that thiophene and furan N-benzyl substituted systems exhibit greater intermolecular interactions than their alkylated analogues ($\Delta E_{CP}$ = -65.45/-74.47 and -72.00/-78.53 kJ mol$^{-1}$ for ***TADPP***/***TBDPP*** and ***FADPP***/***FBDPP*** respectively). Removal of the alkyl or benzyl groups was observed to lead, in all cases to a decrease in the stabilisation of these π-π dimer pairs. This decrease was observed to be more significant on removing the benzyl groups in both thiophene and furan substituted systems ($\Delta E_{CP}$ = -65.45/-51.13, -74.47/-27.26, -72.00/-56.58 and -78.53/-45.11 kJ mol$^{-1}$ for ***XYDPP***/**XDPP** dimer pairs of ***TADPP***, ***TBDPP***, ***FADPP*** and ***FBDPP*** respectively), which we relate to a greater number of intermolecular H-bonding interactions for the N-benzyl derivatives as illustrated in Figure 5. Whereas, intermolecular electrostatic interactions between electropositive methylene hydrogen atoms and electronegative carbonyl oxygens were observed in ***FADPP*** and ***FBDPP*** (separated by 2.82 and 2.86 Å respectively), additional intermolecular H-bonding interactions were also observed in ***FBDPP*** between the electronegative furan oxygen atoms and the electropositive methylene hydrogen atoms, located at a distance of 2.75 Å and facilitated by the larger displacement of the monomers in the dimer pairs along the short molecular axis (vide supra). In turn, the equally large destabilisation computed for the ***TBDPP*** dimer pair, produced as a result of removal of the benzyl groups can be rationalised by a closer (H---O = 2.37 and 2.89 Å for ***TBDPP*** and ***TADPP*** respectively) intermolecular H-bonding interaction between the methylene hydrogen atoms and the electronegative carbonyl oxygens. Lastly, it was observed that in line with phenyl based systems, thiophene and furan containing structures also exhibit a greater destabilisation of N-alkyl substituted dimer pairs on removal of the core rings ($\Delta E_{CP}$ =-59.94/-10.90, -70.12/-28.58, -65.45/-18.95, -74.47/-35.48, -72.00/-24.72 and -78.53/-34.25 kJ mol-1 for ***XYDPP***/**YDPP** dimer pairs of ***PADPP***, ***PBDPP***, ***TADPP***, ***TBDPP***, ***FADPP*** and ***FBDPP*** respectively) This behaviour is associated to an optimised thiophene/furan-DPP core interaction in the alkylated systems facilitated by their closer alignment along the short molecular axis unlike that observed in the benzylated analogues (vide supra).

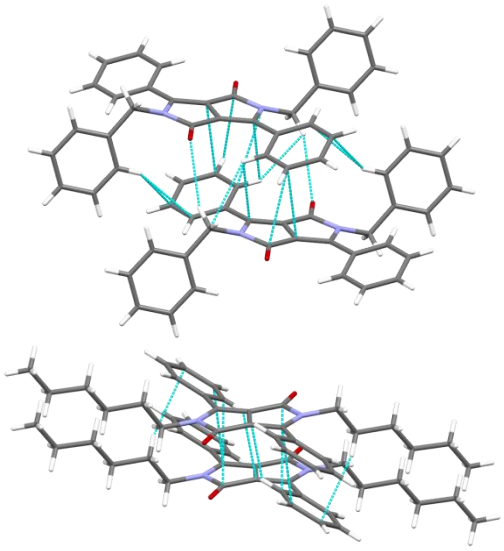

**Figure 4** Capped stick representation of π-π stacking dimer pair of ***PBDPP*** (top) and ***PADPP*** (bottom), with illustrated close interatomic contacts.

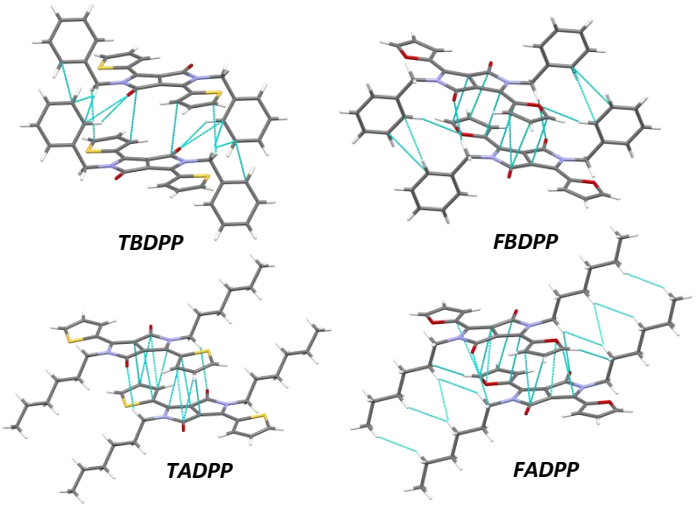


**Figure 5** Capped stick representation of π-π stacking dimer pair of ***FADPP***, ***FBDPP***, ***TADPP*** and ***TBDPP***, with illustrated close interatomic contacts

### Charge transfer integrals for π-π stacking dimer pairs.

In light of the crucial role of electronic coupling in defining the efficiency of charge transfer in organic semiconductors, we determined hole and electron transfer integrals, $t_{h/e}$, for the π-π stacking dimer pairs of the six reported systems.[5-7] To explore the influence of substitution on dictating their transport behaviour, $t_{h/e}$ were also computed for a series of systematically cropped dimer pairs (Table 4). In all cases, transfer integrals were determined using the energy splitting in dimer methodology (ESI), as reported by us previously.[28, 29, 31, 32, 44]

**Table 4** Computed hole ($t_h$) and electron ($t_e$) transfer integrals for modified and unmodified π-π stacking dimer pairs

| | $t_h/t_e$ / kJ mol$^{-1}$ | | | |
|---|---|---|---|---|
| **System** | ***XYDPP*** | **XDPP** | **YDPP** | **DPP** |
| ***PADPP*** | 1.71/1.52 | 1.29/1.16 | 0.59/.28 | 0.56/.41 |
| ***PBDPP*** | 10.69/6.13 | 9.78/5.95 | 3.20/5.77 | 4.67/4.89 |
| ***TADPP*** | 7.78/15.54 | 7.71/14.98 | 5.66/6.62 | 7.88/5.69 |
| ***TBDPP*** | 6.00/5.47 | 5.39/4.84 | 5.38/3.40 | 5.65/3.21 |
| ***FADPP*** | 2.78/20.40 | 3.20/19.90 | 5.87/3.00 | 8.74/2.95 |
| ***FBDPP*** | 4.53/15.05 | 4.79/14.89 | 3.26/9.31 | 3/17/9.13 |

Via analysis of the computed $t_{h/e}$ we conclude that the π-π stacking dimer pair of ***PBDPP*** exhibits the largest hole transfer integral for all of the investigated systems, with electronic coupling approaching that of rubrene ($t_h$ = 10.69 and 12.40 kJ mol$^{-1}$ for π-π dimer pairs of ***PBDPP*** and rubrene respectively). Of considerable interest to us was the significant deterioration in the magnitude of the transfer integrals for both holes and electrons upon alkyl substitution on the lactam nitrogen atoms with phenyl substitution ($t_h/t_e$ = 10.69/6.13 and 1.71/1.52 kJ mol$^{-1}$ for π-π dimer pairs of ***PBDPP*** and ***PADPP*** respectively), which can be readily accounted for as a consequence of the dimer stacking displacements exhibited by these systems (vide supra) and subsequent lower wavefunction overlap as illustrated in Figure 6. On progression from phenyl to thiophene based architectures this scenario was reversed, with a greater hole and electron transfer integral observed for the alkylated thiophene member compared with its benzylated equivalent ($t_h/t_e$ = 6.00/5.47 and 7.78/15.54 kJ mol$^{-1}$ for π-π dimer pairs of ***TBDPP*** and ***TADPP*** respectively).

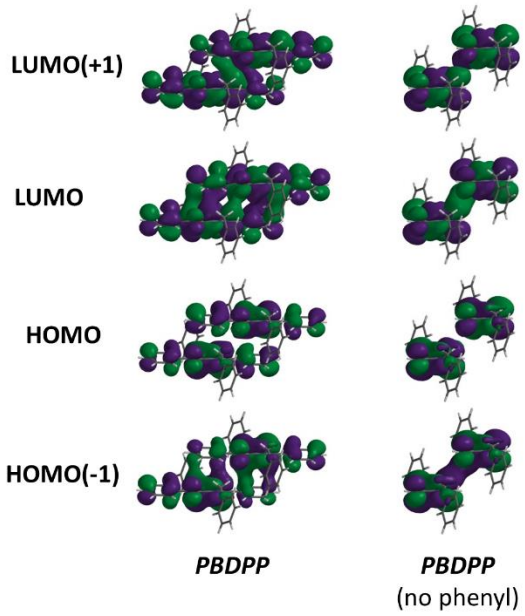


**Figure 6** Illustration of the supramolecular orbitals of ***PADPP*** and ***PBDPP***

The computed $t_e$ identified for the π-π stacking dimer pair of ***TADPP*** is considerable, and denotes a two-fold increase from that computed by us for rubrene ($t_e$ = 15.54 and 7.50 kJ mol$^{-1}$ for π-π stacking dimer pairs of ***TADPP*** and rubrene respectively). Remarkably, replacement of alkyl for benzyl substituents on the lactam nitrogen atoms in the thiophene systems afforded a dramatic decrease in the computed $t_e$, which we ascribe to the increased displacement along the short molecular axis upon benzyl substitution (vide supra) and associated decrease in LUMO wavefunction overlap, illustrated in Figure 7. In the benzylated thiophene analogue ***TBDPP***, ambipolar charge transfer is predicted, with notable $t_h/t_e$ anticipated for the π-π stacking dimer pair ($t_h/t_e$ = 6.00/5.47 kJ mol$^{-1}$). We compute the largest electron transfer integral in any of the systems for the π-π dimer pair of ***FADPP*** ($t_h/_e$ = 2.78/20.40 kJ mol$^{-1}$). Unlike the scenario described for ***TABDPP***/***TBDPP*** however, we also report a large computed $t_e$ for the π-π stacking dimer pair of the benzylated analogue, ***FBDPP***, consistent with a reduced short molecular axis shift observed in the furan based system upon benzyl substitution (Δy = 0.05/3.26 and 0.15/1.78 Å for π-π dimer pairs of ***TADPP***/***TBDPP*** and ***FADPP***/***FBDPP*** respectively). In conclusion, it is clear that systematic substitution of the lactam nitrogen atoms, as well as of the core aryl rings can result in significant changes to intermolecular displacements and hence charge transfer properties in these DPP single crystals.

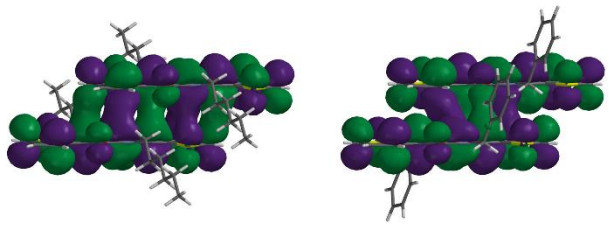

**Figure 7** Illustration of the LUMO supramolecular orbitals of ***TADPP*** (left) and ***TBDPP*** (right).

To broaden our understanding of substituents effects in controlling the charge transfer properties of the crystal structures described, we computed hole and electron transfer integrals for a series of systematically cropped dimer pairs. The effect of N-substitution on the computed transfer integrals can be understood by comparison of ***XYDPP*** and **XDPP** dimers. We report negligible changes on removal of either alkyl or benzyl groups, which is in line with the very limited extension of the HOMO/LUMO wavefunction onto the N-substituents, as previously reported by us. In turn, significant differences were observed on progression from ***XYDPP*** to artificially generated **YDPP** dimer pairs. In all cases, a reduction of the computed $t_h/t_e$ was observed, with the exception of the hole transfer integral for ***FADPP*** ($t_h$ = 2.78 and 5.87 kJ mol$^{-1}$ for dimer pairs ***XYDPP*** and **YDPP** of ***FADPP*** respectively). Via inspection of the computed supramolecular orbitals, we associate this behaviour to a decrease/increase in the bonding/anti-bonding character of the HOMO(-1) and HOMO supramolecular orbitals respectively (ESI). In addition, of interest to us was reversal of the $t_h/t_e$ values computed for our flagship hole transport architecture, ***PBDPP***, on progression from ***XYDPP*** to **YDPP** ($t_h/t_e$ = 10.69/6.13 and 3.20/5.77 kJ mol$^{-1}$ for dimer pairs **XYDPP** and **YDPP** of ***PBDPP*** respectively). In short, we observed a more significant decrease of $t_h$ compared to $t_e$ on removal of the core phenyl rings, and hence a reversal in magnitude of the charge transfer integrals; this behaviour associated to an increase in the antibonding character of the ungerade LUMO(+1) on progression from ***XYDPP*** to **YDPP** in ***PBDPP*** (ESI).

### Inner-sphere intermolecular interactions and reorganisation energies

Inner-sphere hole and electron transfer reorganisation energies, $\lambda_{e/h}$, were estimated for each of the investigated crystal structures via their non N-substituted analogues, **PDPP**, **TDPP** and **FDPP** (Figure 8), by revisiting our previously reported methodology (ESI) for the determination of inner-sphere reorganisation energies in **PDPP** (**$H_2$DPP** in the original publication).[60]

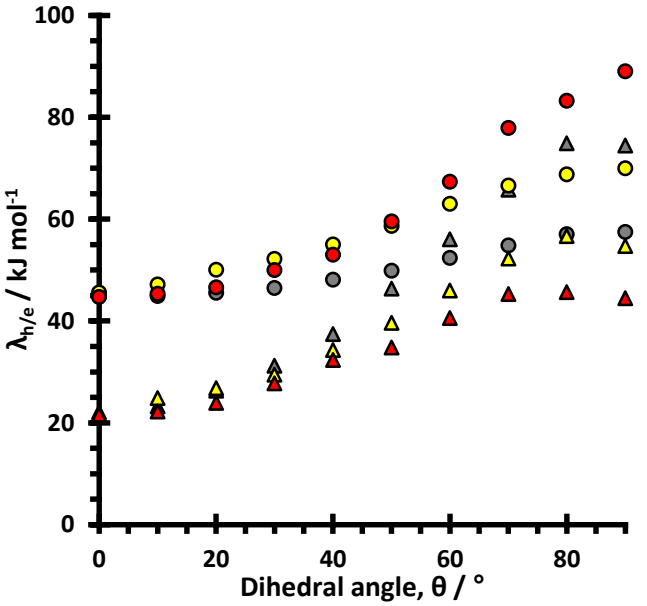


**Figure 8** Computed inner-sphere reorganisation energies towards hole, $\lambda_h$ (filled circles) and electron, $\lambda_e$ (filled triangles) transfer for **PDPP** (grey), **TDPP** (yellow) and **FDPP** (red)

We have shown that for the **PDPP** model system, $\lambda_e$ manifests a larger response to changes in the torsion of the core phenyl rings, and for dihedral angles greater than ca. 60° a reversal of the inner-sphere reorganisation energies was computed with $\lambda_e > \lambda_h$.[27] This characteristic behaviour is attributed to an out-of-plane rearrangement primarily associated to the C-C linker between the DPP core and the core phenyl rings. The structural re-arrangement was

observed to be greater in the radical anion species and to be minimal in radical cation geometries compared with their neutral equivalent ($\Delta\eta$ = 29.33/0.11° on going from neutral to radical anion/cation optimised geometries at $\theta$ = 90°). Rather surprisingly to us, analogous model systems for **TDPP** and **FDPP** do not exhibit this behaviour, whereby $\lambda_h$ dominates the progression for all of the investigated dihedral angles. Importantly, we observe that for dihedral angles lower than ca. 35 °, which are commonly observed in DPP single crystal structures, computed inner-sphere reorganisation energies for **PDPP**, **TDPP** and **FDPP** are comparable. Furthermore, as the twist of the rings with respect to the DPP core is increased further than 35 °, larger differences are observed, with the highest electron and hole transfer reorganisation energies computed for phenyl and furan based systems respectively. Via analysis of the optimised geometries, we associate this behaviour to out-of-plane re-arrangement around the C-C link between DPP core and core aryl rings on progression from neutral to radical species, which exhibit a linear relationship with respect to their respective computed inner-sphere reorganisation energies. We conclude, for systems characterised by dihedral angles lower than ca 30 °, which are most common in DPP single crystal structures such as those discussed herein, that inner-sphere reorganisation energies should not play a differentiating role amongst phenyl, thiophene or furan architectures in charge transfer processes within the hopping regime.

## Conclusions

In summary, we find that for all of the systems examined, N-benzylation ensures the largest π-π stacking interaction energies, $\Delta E_{CP}$, and therefore should be considered over conventional alkyl substitution for solubilisation and crystal engineering of DPP small molecules. For optimal electron transport, we propose that N-alkyl and N-benzyl furan based DPP OSCs should be explored further, owing to their high computed electron transfer integrals, $t_e$ and lower reorganisation energies, $\lambda_e$. Surprisingly to us and contrary to popular misconception, we have demonstrated that hole transport is predicted to be optimal in the twisted phenyl substituted N-benzyl DPP. Therefore, despite a more significant dihedral angle in this structure (20.60 °) compared to both alkyl and benzyl thiophene (10.04 and 3.50 °) and furan (0.86 and 1.00 °) equivalents, N-benzyl substitution of the phenyl DPP is effective in facilitating close cofacial π-π stacking interactions between the conjugated monomers, enhancing their HOMO wavefunction overlap and maximising hole transfer integrals, $t_h$. In comparing computed reorganisation energies, $\lambda_{h/e}$, across the series we report that $\lambda_e < \lambda_h$ for phenyl, thiophene and furan DPPs, and as a result, greater electron charge mobility over hole might be expected from these structures in the absence of external environmental influences. As highlighted previously, N-substitution increases $\lambda_e$ for phenyl DPPs relative to their thiophene and furan equivalents, owing to the contribution of significant torsional relaxation to the reorganisation energy of the phenyl radical anion; further supporting the viability of furan and thiophene based DPP single crystals in processes that involve electron transport. Notably, we find that $\lambda_h$ does not significantly vary between phenyl and heteroaromatic substituents; underpinning our assertion that contrary to popular belief, studies of phenyl N-benzyl DPP single crystals, especially in hole conducting OFET devices are in fact warranted. Accordingly, we anticipate our results should be of broad interest to those developing crystalline organic electronic materials, particularly those based around the DPP architecture.

## Experimental

Full details regarding the preparation, characterisation, crystallographic analysis and theoretical modelling of reported compounds are available in the electronic supplementary information.

## Acknowledgements

C.J.M. acknowledges the EPSRC for funding under the First Grant Scheme (EP/J011746/1) and the University of the West of Scotland for Ph.D. funding for G.M.

## Notes and references

1. H. Chung and Y. Diao, *J. Mat. Chem. C*, 2016, **4**, 3915-3933.
2. P. M. Beaujuge and J. M. J. Frechet, *J. Am. Chem. Soc.*, 2011, **133**, 20009-20029.
3. M. Mas-Torrent and C. Rovira, *Chem. Rev.*, 2011, **111**, 4833-4856.
4. C. Wang, H. Dong, W. Hu, Y. Liu and D. Zhu, *Chem. Rev.*, 2011, **112**, 2208-2267.
5. V. Coropceanu, Y. Li, Y. Yi, L. Zhu and J.-L. Brédas, *MRS Bull.*, 2013, **38**, 57-64.
6. L. Wang, G. Nan, X. Yang, Q. Peng, Q. Li and Z. Shuai, *Chem. Soc. Rev.*, 2010, **39**, 423-434.
7. A. Troisi, *Chem. Soc. Rev.*, 2011, **40**, 2347-2358.
8. J. L. Bredas, J. P. Calbert, D. A. da Silva and J. Cornil, *Proc. Natl. Acad. Sci.U.S.A*, 2002, **99**, 5804-5809.
9. V. Coropceanu, J. Cornil, D. A. da Silva Filho, Y. Olivier, R. Silbey and J.-L. Bredas, *Chem. Rev.*, 2007, **107**, 926-952.
10. J. S. Ha, K. H. Kim and D. H. Choi, *J. Am. Chem. Soc.*, 2011, **133**, 10364-10367.
11. D. Cortizo-Lacalle, S. Arumugam, S. E. T. Elmasly, A. L. Kanibolotsky, N. J. Findlay, A. R. Inigo and P. J. Skabara, *J. Mater. Chem.*, 2012, **22**, 11310-11315.
12. Z. Chen, M. J. Lee, R. S. Ashraf, Y. Gu, S. Albert-Seifried, M. M. Nielsen, B. Schroeder, T. D. Anthopoulos, M. Heeney, I. McCulloch and H. Sirringhaus, *Adv. Mater.*, 2012, **24**, 647-+.
13. J. Lee, S. Cho, J. H. Seo, P. Anant, J. Jacob and C. Yang, *J. Mater. Chem.*, 2012, **22**, 1504-1510.

 

14. W. Hong, B. Sun, H. Aziz, W.-T. Park, Y.-Y. Noh and Y. Li, *Chem. Commun.*, 2012, **48**, 8413-8415.
15. J. Liu, Y. Sun, P. Moonsin, M. Kuik, C. M. Proctor, J. Lin, B. B. Hsu, V. Promarak, A. J. Heeger and N. Thuc-Quyen, *Adv. Mater.*, 2013, **25**, 5898-5903.
16. H. Bronstein, Z. Chen, R. S. Ashraf, W. Zhang, J. Du, J. R. Durrant, P. S. Tuladhar, K. Song, S. E. Watkins, Y. Geerts, M. M. Wienk, R. A. J. Janssen, T. Anthopoulos, H. Sirringhaus, M. Heeney and I. McCulloch, *J. Am. Chem. Soc.*, 2011, **133**, 3272-3275.
17. S. Qu, W. Wu, J. Hua, C. Kong, Y. Long and H. Tian, *J. Phys. Chem. C*, 2010, **114**, 1343-1349.
18. S. Qu and H. Tian, *Chem. Commun.*, 2012, **48**, 3039-3051.
19. S. Qu, C. Qin, A. Islam, Y. Wu, W. Zhu, J. Hua, H. Tian and L. Han, *Chem. Commun.*, 2012, **48**, 6972-6974.
20. P. Data, A. Kurowska, S. Pluczyk, P. Zassowski, P. Pander, R. Jedrysiak, M. Czwartosz, L. Otulakowski, J. Suwinski, M. Lapkowski and A. P. Monkman, *J. Phys. Chem. C*, 2016, **120**, 2070-2078.
21. J. Kwon, H. Na, A. K. Palai, A. Kumar, U. Jeong, S. Cho and S. Pyo, *Synth. Met.*, 2015, **209**, 240-246.
22. S. Arumugam, D. Cortizo-Lacalle, S. Rossbauer, S. Hunter, A. L. Kanibolotsky, A. R. Inigo, P. A. Lane, T. D. Anthopoulos and P. J. Skabara, *ACS Applied Materials and Interfaces*, 2015, **7**, 27999-28005.
23. S. G. Surya, S. S. Nagarkar, S. K. Ghosh, P. Sonar and V. Ramgopal Rao, *Sensors and Actuators, B: Chemical*, 2016, **223**, 114-122.
24. P. Homyak, Y. Liu, F. Liu, T. P. Russel and E. B. Coughlin, *Macromolecules*, 2015, **48**, 6978-6986.
25. X. Guo, S. R. Puniredd, B. He, T. Marszalek, M. Baumgarten, W. Pisula and K. Muellen, *Chem. Mater.*, 2014, **26**, 3595-3598.
26. A. B. Tamayo, X.-D. Dang, B. Walker, J. Seo, T. Kent and T.-Q. Nguyen, *Appl. Phys. Lett.*, 2009, **94**.
27. J. Calvo-Castro, C. J. McHugh and A. J. McLean, *Dyes and Pigments*, 2015, **113**, 609-617.
28. J. Calvo-Castro, M. Warzecha, I. D. H. Oswald, A. R. Kennedy, G. Morris, A. J. McLean and C. J. McHugh, *Cryst. Growth Des.*, 2016, **16**, 1531-1542.
29. J. Calvo-Castro, M. Warzecha, A. R. Kennedy, C. J. McHugh and A. J. McLean, *Cryst. Growth Des.*, 2014, **14**, 4849-4858.
30. J. Calvo-Castro, M. Warzecha, A. J. McLean and C. J. McHugh, *Vib. Spectrosc*, 2016, **83**, 8-16.
31. J. Calvo-Castro, G. Morris, A. R. Kennedy and C. J. McHugh, *Cryst. Growth Des.*, 2016, **16**, 5385-5393.
32. J. Calvo-Castro, G. Morris, A. R. Kennedy and C. J. McHugh, *Cryst. Growth Des.*, 2016, **16**, 2371-2384.
33. M. Warzecha, J. Calvo-Castro, A. R. Kennedy, A. N. Macpherson, K. Shankland, N. Shankland, A. J. McLean and C. J. McHugh, *Chem. Commun.*, 2015, **51**, 1143-1146.
34. J. Vura-Weis, M. A. Ratner and M. R. Wasielewski, *J. Am. Chem. Soc.*, 2010, **132**, 1738-+.
35. S. E. Wheeler, A. J. McNeil, P. Müller, T. M. Swager and K. N. Houk, *J. Am. Chem. Soc.*, 2010, **132**, 3304-3311.
36. C. B. Nielsen, M. Turbiez and I. McCulloch, *Adv. Mater.*, 2013, **25**, 1859-1880.
37. J. Dhar, N. Venkatramaiah, A. Anitha and S. Patil, *J. Mat. Chem. C*, 2014, **2**, 3457-3466.
38. J. Dhar, D. P. Karothu and S. Patil, *Chem. Commun.*, 2015, **51**, 97-100.
39. C. Fu, F. Belanger-Gariepy and D. F. Perepichka, *CrystEngComm*, 2016, **18**, 4285-4289.
40. A. B. Tamayo, M. Tantiwiwat, B. Walker and T.-Q. Nguyen, *The Journal of Physical Chemistry C*, 2008, **112**, 15543-15552.
41. R. Sevincek, S. Celik, M. Aygun, S. Alp and S. Isik, *Acta Crystallographica Section E*, 2010, **66**, o1546.
42. M. A. Naik, N. Venkatramaiah, C. Kanimozhi and S. Patil, *J. Phys. Chem. C*, 2012, **116**, 26128-26137.
43. D. A. da Silva, E. G. Kim and J. L. Bredas, *Adv. Mater.*, 2005, **17**, 1072-+.
44. J. L. Bredas, D. Beljonne, V. Coropceanu and J. Cornil, *Chem. Rev.*, 2004, **104**, 4971-5003.